Grain size affecting the deformation characteristics via micro-injection upsetting

Walaa Abd-Elaziem[a], Mohsen A. Hassan[b], Takehiko Makino[c] and Atef Hamada[d]

[a]Department of Mechanical Design and Production Engineering, Faculty of Engineering, Zagazig University, Zagazig, Egypt; [b]Egypt-Japan University of Science and Technology, New Borg El-Arab City, Egypt; [c]Department of Mechanical Engineering, Nagoya Institute of Technology, Nagoya, Japan; [d]Kerttu Saalasti Institute, University of Oulu, Nivala, Finland

ABSTRACT

The micro-injection upsetting (MIU) experiments of commercially pure aluminium have been conducted on two groups of specimens with different grain structures. One group is of coarse grain (CG, undeformed) and the other group is of fine grain (FG) achieved via the 4th pass equal channel angular pressing in micro-meso/scale. The two groups were further processed by micro/meso-scale extrusion before conducting MIU for fabricating tiny pins. Micro-upsetting test of the tiny pins showed that the material has a good isotropic flow forming and is free of unde- sirable defects comparing with the CG counterparts, which can be ascribed to the decreasing of grain boundary strengthening effect in the case of FG structure.

ARTICLE HISTORY
Received 22 April 2021
Revised 29 July 2021
Accepted 1 August 2021

KEYWORDS
Refinement; severe plastic deformation; size effects; friction; microstructure

Introduction

Driven by rising demand from the miniature/micro-components for micro-electro-mechanical systems (MEMS) at an unprecedented rate, continuous research is going on to improve the productivity and the quality of micro-products. Microforming is considered as one of the most important micro-manufacturing methods since it has the distinct advantages of mass production capability with controlled quality, repeatability, effective material utilisation, and low cost.[1–5].

Despite its potential, the knowledge of tool design and fabrication methods is not established yet. The main reasons for this are the departure of the mature theory applicable to macro-scale forming, i.e. conventional forming, and increasing process scatter, which causes difficulties in controlling the quality of micro-formed parts. This phenomenon is called the 'size-effect' which causes some differences in the basic manufacturing characteristics applied in macro-forming when the specimen geometrical dimensions are scaled down to micro-scale [6,7].

As a result of the ongoing trend of need for miniaturisation, the coarse-grained materials (CG) that have a size of its grains typically ranging from ten to several hundreds of microns do not turn into a small scale as compared by the dimension characteristics of the tiny parts. In other words, if the specimen has a few grains in the deformation zones then the response of the individual grains to the applied forces would cause substantial variations in the deformation behaviour that make scattering in the mechanical properties [8–10]. It follows, therefore, that the size effect is critical and must be taken into consideration in the fabrication of micro-parts.

Addressing this issue, Wang et al.[11] demonstrated that the material grain size has a decisive effect on the microformability of the materials. Rosochowski et al. [12] performed micro-extrusion on two differ- ent structures of Al alloy, CG and ultrafine-grained (UFG) by macro-scale equal channel angular pressing (3D-ECAP) die. They found that using UFG structure in microforming leads to more uniform products with improved mechanical properties compared to its CG counterpart.

Xu et al. [8] investigated the deformation behaviour via micro-compression deformation on two different structures of high-purity aluminium, coarse-grained (CG), and UFG. They reported that strain softening in the flow stress curves was taken place after exhibiting strain hardening with grain refining.

Durst et al. [13] successfully achieved nano and micro-imprinting on the material surface of nanocrystalline and UFG Ni. Kim et al. [14] processed a high-quality pyramid pattern and micro-V grooves through superplastic deformation of UFG magnesium alloy.

From the above literature, it can be stated that the grain size is a decisive factor that can determine the limiting size of the geometrical shapes of the micro-parts. In practice, this means that FG structure materials are attractive for utilising in the fabrication process of micro-forming.

Walaa Abdel-Aziem walaa.abdelaal@ejust.edu.eg Department of Mechanical Design and Production Engineering, Faculty of Engineering, Zagazig University, P.O. Box 44519, Zagazig, Egypt

Recently, the researchers revealed the potential for utilising FG materials in microforming processes at ambient and elevated temperatures [8,15]. However, only very limited studies are available on the deformation behaviour during the processing of micro- parts when the grain structure is refined into a very small diameter size despite these challenges are attract-ing the attention of the materials science researchers [16–18].

It is well known that FG materials can be easily produced to large bulk specimens via the techniques of severe plastic deformation, such as ECAP [19–21], cyclic extrusion and compression (CEC) [22,23], and high-pressure torsion [24,25]. However, to the best of our knowledge, these techniques were applied in macro-scale, i.e. die channel diameter > 5 mm. Thus, the processed specimens by these traditional techniques have to be further formed, machined, etched, etc., to reach the small size needed to advance into micro-forming techniques to produce net micro-products.

Thus, in our previous works [26,27], a miniaturised version of micro/meso-scale ECAP (MMSECAP), as well as micro/meso-scale extrusion (MMSE) dies as new techniques for fabricating miniaturised parts, were designed and implemented for improving the feasibility of micro-components manufacturing. Additionally, the microstructural evolution of the samples subjected to ECAP as a pre-processing method followed by micro/meso-extrusion processing to improve the grain structure of AA1070 alloy was investigated. Besides, the results of the tensile properties for the processed samples via a special tensile test machine were detailed in the previous work.

This work aims to study the micro-upsetted behavi our of commercial aluminuim Al 1070 alloy hav- ing two different grain structures, i.e. CG and FGin which the latter was attained firstly by process-ing MMSECAP in order to attain fine-grain structure and then followed by cold extrusion. The microstruc- tural evolution through the multi-processing stages and surface quality after micro-upsetted were stud-ied as well as the surface deformation behaviour for both CG and FG aluminuim, i.e. friction factors were proposed.

Experimental study

In this study, pure Al 1070 was selected for its widespread use in electrical and electronic applications to evaluate the anisotropy of the final deformation using injection upsetting on a micro-scale. The alloy was received as long rods of 1.5 ϕ mm $\times$ 300 mm. The as-received rods were subjected to a short heating cycle up to 350 °C at a heating rate of 1.5°C s^{-1}, then cooled to room temperature to get rid of machining processing effects.

Two sets of specific processing were performed after the annealing process to get two different grain structures, i.e. CG and UFG. The first processing group was extruded from a diameter of 1.5 to 1 mm (CG) and the other group is subjected to ECAP before the extrusion process (FG).

The MMSECAP die used in this study has a distinct design in which the two separated rectangular halves with the same channel diameter of 1.5 mm are assembled at an angle of 45° as can be seen in Figure 1(a). This design can produce a smooth surface specimen without the formation of any cracks or burrs that can be unavoidably formed during processing the specimens via traditional ECAP as the two halves of the die are cutting along the channels. A cover plate is implemented to avoid detaching the two parts of the ECAP die. More details about MMSECAP die and the typical appearance of the specimens processed by MMSECAP can be found in our previous study [28].

Rods were cut for ECAP with original diameters of 1.5 mm and lengths of 11 mm. The prepared specimens were conducted up to the 4th ECAP pass using route B_C, i.e. the specimens underwent a 90° rotation counter-clockwise between consecutive passes around their longitudinal direction. This route was selected in this investigation because it is reported that route B_C is an effective route in refining the grain structure in the 90° die [29].

Following MMSECAP, rods were cut into lengths of 6 mm for the subsequent extrusion process to fabricate tiny pins. The extrusion process was conducted at room temperature for the annealed specimens (CG) and only the specimens subjected to the 4th ECAP pass (FG). To avoid deburring for the material dur-ing extrusion, the two halves of the die were cut horizontally as in the MMSECAP die, not as usual in cutting vertical, see Figure 1(a). Therefore, an additional specimen had to be prepared for completing the extrusion process because the punch cannot push till the end of the die. For instance, after a first specimen was pushed to half of its initial length (3 mm), a second specimen was inserted and pressed also to about half of its length, at that time the first specimen was totally extruded. For the as-received rods after annealing, henceforward designated the 'Undeformed' condition and for the as-received rods after annealing followed by MMSE, henceforward designated the 'Undeformed + Extr.' condition. Finally, for the annealing rods after MMSECAP through four passes at room temperature followed by MMSE, henceforth designated the "Undeformed + ECAP + Extr." condition.

All the processes (ECAP and extrusion) were conducted under a displacement rate of 1 mm min^{-1}. This pressing rate in this work is reasonable to ensure there is no significant effect from any heating of the specimen during processing.

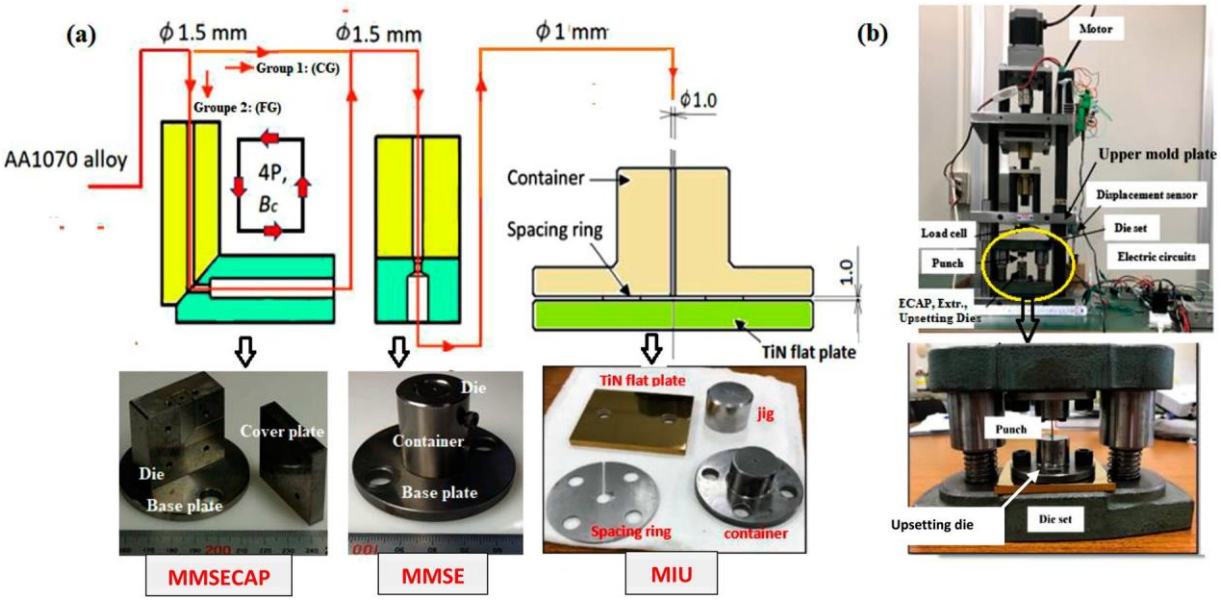

Figure 1. (a) Schematic illustration of the sequence of the applied processes in this investigation with the corresponding typical implemented dies, and (b) The employed experimental setup [30]. MMSECAP symbolises micro/meso-scale ECAP, MMSE symbolises micro/meso-scale extrusion, and MIU represents micro-injection upsetting.

The two different grain structures, CG (Undeformed + Extr.) and FG (Undeformed + ECAP + Extr.), then underwenta final processing step of micro-injection upsetting (MIU) (see Figure 1(a)). The injection upsetting apparatus consists of three main parts, i.e. container (upper die), spacing ring, and flat plate. The spacing ring which has a thickness of 1 mm was used to make a gap between the upper die and the flat plate. The flat plate was coated by TiN with a surface roughness of Ra = 0.01 μm, measured at Makino Laboratory at Nagoya Institute of Technology, Nagoya, Japan. The appearance of the actual experimental platform can be shown by the high magnification of the zone highlighted by the yellow circle in Figure 1(b).

All the initial specimens prepared for the upsetting test have a dimension of 1 mm diameter with 8 mm in height. The opposite ends of the test specimens were polished by grinding paper using a jig to maintain the perpendicularity and to facilitate the handling of the specimens. Then, both the specimens and the coated plate were polished with a buff and 1 μm diamond spray followed by a cleaning process using an ultrasonic device (acetone, the cleaning solution). In the injection upsetting process, the specimens were pressed through the channel of the upper die to inject the gap between the upper die and the TiN plate. The injection upsetting specimens were pressed up to 2 mm height (stroke) from the total specimen height (8 mm) at room temperature.

All the aforementioned processing, i.e. MMSECAP, MMSE, and MIU were performed on a servo-press machine witha5 kN load cell and a displacement gauge as can see in Figure 1(b).

Microstructural examinations were characterised by electron backscatter diffraction (EBSD, JEOl JSM-7001F). For EBSD, specimens were cut parallel to the extrusion direction, they were mechanically ground on standard silicon carbide papers, then finally polished with 0.04 μm colloidal alumina (OP-S). EBSD measurements were performed at 15 kV, a tilt angle of 70° and a scan step of 0.3 μm on a zone of 150 μm × 150 μm.

Microstructural observations in the longitudinal direction were performed also by transmission electron microscopy (TEM) on specimens exposed to MMSECAP deformation to reveal the hard-to-notice grain refinement of EBSD. TEM specimens were prepared with a focused ion beam technique in which a thickness of 200 nm was produced.

Results and discussion

Microstructural evolution during MMSECAP/MMSE

The broad aspects of microstructure evolution dur-ing MMSECAP/MMSE were displayed in our previous work of the present authors [26,27]. For suitability, the main issues of this process are shortly summarised here. Figure 2 shows the EBSD microstructure maps of Al 1070 alloy before and after MMSECAP passes. In the maps, the thin and thick black lines from these maps indicate the location of low-angle grain boundaries (LAGBs, $2° \leq \theta \leq 15°$) and high-angle grain boundaries (HAGBs, $\theta \geq 15°$), respectively. It is worth noting that the LAGBs are subgrain boundaries which are composed of an array of dislocations. For simplicity, only HAGBs are shown in thick lines. Figure 2(a) shows that the microstructure of the undeformed material displays equiaxed grain morphology with an average grain size of ~ 20.4 μm and an average misorientation angle of 19.57°, i.e. ≥ 15°. After the 1st ECAP pass, it is

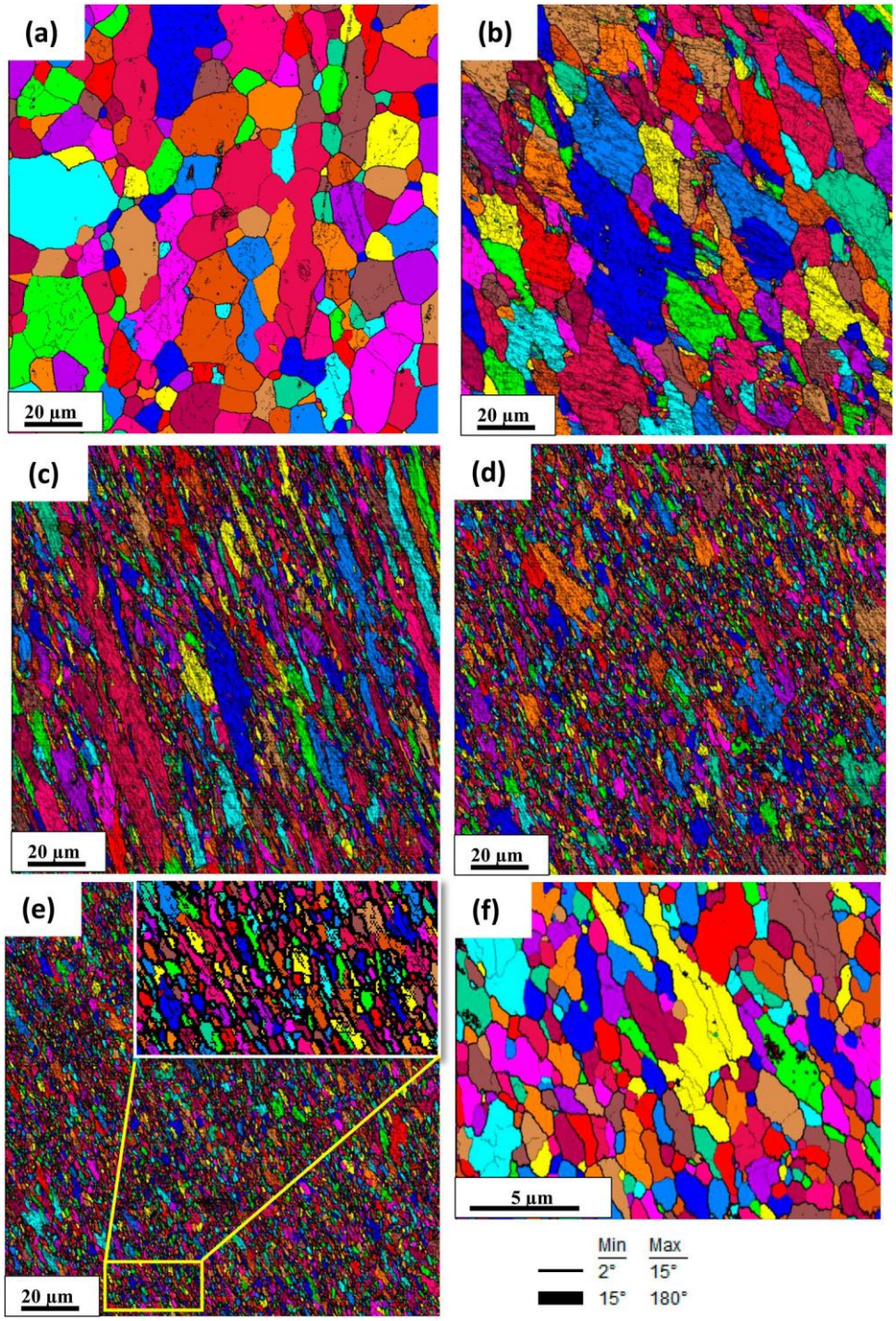

Figure 2. EBSD orientation maps: (a) undeformed; (b) one ECAP pass; (c) two ECAP passes; (d) three ECAP passes; (e) four ECAPpasses; and (f) High-magnification EBSD map for the 4th ECAP pass on an area of 20 µm × 20 µm [26,27].

found that a heterogeneous microstructure mostly consists of elongated grains towards the shearing direction (see Figure 2(b)). Moreover, the microstructure consists mainly of a large fraction of LAGBs as already shown in Figure 2(b), qualitatively.

As the MMSECAP deformation proceeds to the fourth pass, more refined grains, Figure 2(e), as compared to the preceding microstructures, i.e. second and third pass. Therefore, notwithstanding relatively rapid grain refinement through early stagesof MMSECAP (Figure 2), the microstructure still has a slightly heterogeneous distribution where some relatively large grains of size ~ 9 µm are demon- strated in the high magnification microstructure of 4thECAP pass (Figure 2(f)). Thus, a significant number of MMSECAP passes are necessary to obtain a reasonably uniform grain structure.

Grain refinement during MMSECAP isa direct consequence of the formation and subsequent evolution of deformation stress-induced boundaries. Figure 3(a,b) show the statistical variations of grain size and the boundary misorientation angle distribution attained from the EBSD analysis after ECAP passes, respectively. It is shown that the average size of the coarse grains in

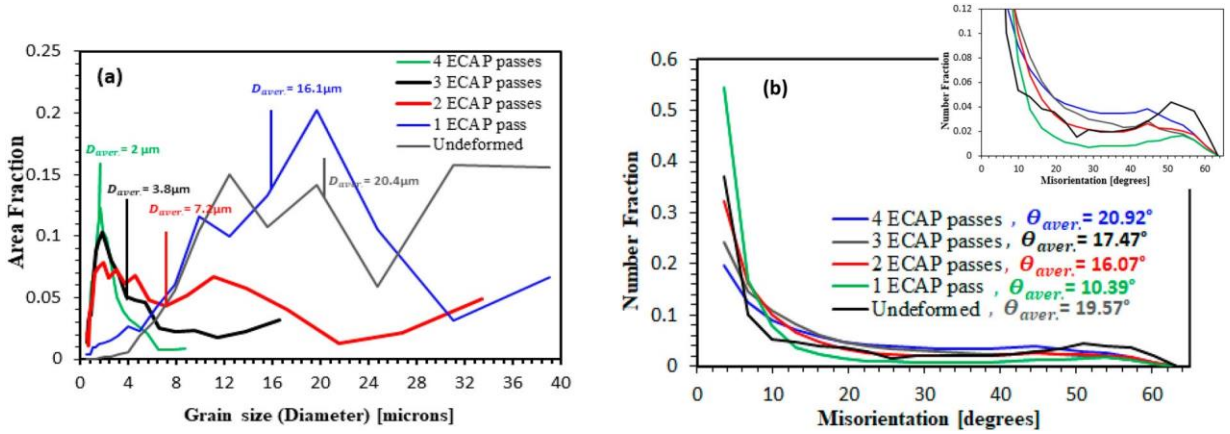

Figure 3. (a) Line grain size distribution and (b) boundary misorientation distribution of Al 1070 aluminium subjected to micro/meso-scale ECAP processing on a plane aligned to the extrusion direction.

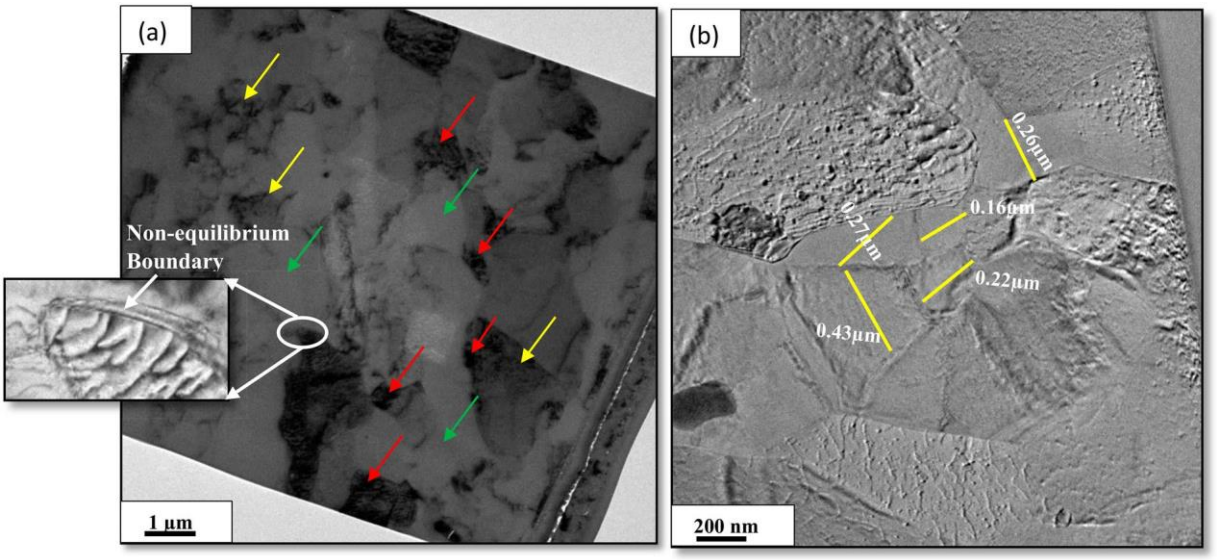

Figure 4. TEM micrographs of (a) 1st pass and (b) 4th pass of the specimens processed by MMSECAP.

the undeformed alloy decreased with an increase in the number of ECAP passes, likely as a consequence of the gradual transformation of LAGBs to HAGBs. The average grain size is about 16.1 μm, 7.2 μm, 3.8 μm, and ~ 2 μm after 1, 2, 3, and 4 passes, consistently. Correspondingly, the average misorientation angle increases from 10.39°, 16.07°, 17.47° to 20.92°.

Compared with the structure of the undeformed specimen, the degree of grain refinement remarkably increased after the 4th ECAP pass, i.e. about ~ 80% of grains fall in the range 1–3 μm (see Figure 3(a)). This is due to the grain subdivision during MMSECAP straining.

The mechanism of grain subdivision [31–34] is mainly ascribed to the dislocation boundaries (dense dislocation walls) [35–37] that rise due to trapping of the dislocations which in turn form subgrains or cell blocks with LAGBs within the interior of grains [37,38]. These boundaries strengthen and eventually evolve into low-angle boundaries (LAGBs, < 15°). With more straining, dislocation activities in the par-ent grains become difficult due to the inhibition of intergranular strains [39]. Therefore, the plastic strain could be accommodated by rotation of these boundaries and increasing the misorientations leading to the formation of higher-angle boundaries (HAGBs, >15°) and subsequently, new finer grains are generated within the initial grains. This is in line with [40] in which the HAGBs are formed by grain subdivision in severely deformed aluminium (Al 1050) processed by ECAP were investigated. Similarly, studies demonstrate that as the number of ECAP passes increases, the fraction of HAGBs increases [41–43]. This results in simultaneously increasing the strength of the material, as well as improving the homogeneity of the microstructure [41]. Delannay et al. [44] studied the grain subdivision on the same previous material via cold rolling to a reduction of 40% by using Orientation Imaging Microscopy (OIM).

For more clarification about the structure, Figure 4 shows the TEM micrograph of the 1st and the 4th passes of MMSECAP processed specimens. After the 1st pass of MMSECAP, it is demonstrated that the structure shows the presence of dislocations inside the deformed

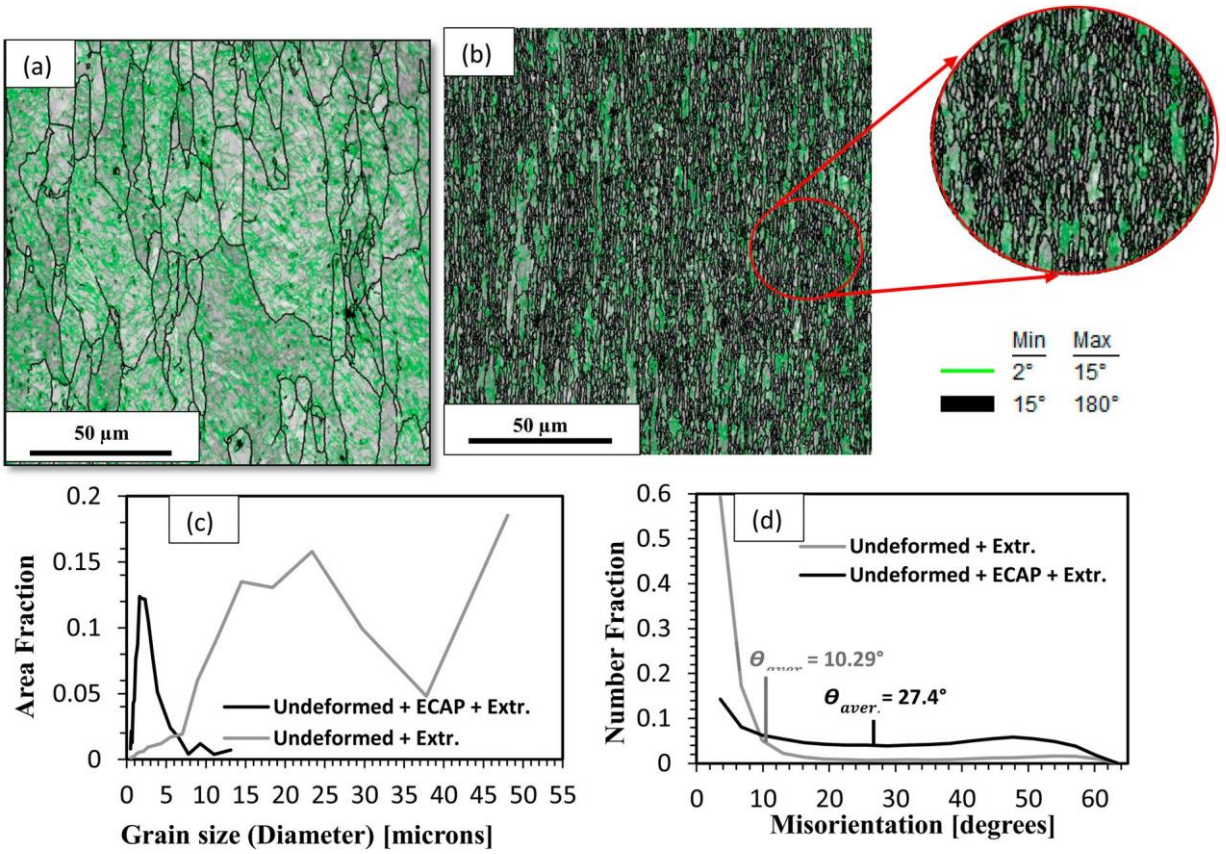

Figure 5. (a,b) Boundary map on the longitudinal direction of the Undeformed + Extr., and Undeformed + ECAP+ Extr., respectively. (c) Line grain size distribution and (d) misorientation angle distribution of the Al specimens processed by MMSE.

grains, see, for instance, there are three types of zones in Figure 4(a). (I) Zones that have almost no dislocations, designated by green rows, (II) zones comprising dislocation tangles and sub-boundaries, showed by yellow rows, and (III) zones consisting of a high density of dislocations which are distributed randomly, indicated by red rows. These dislocations are not presented in the lowest-energy dislocation structure [45,46] which is likely exploited in the formation of the unstableor non-equilibrium grain boundary (Figure 4(a)) and may realign to form equilibrium boundaries. Henceforward, with further deformation, it is likely that these boundaries will be evolved into HAGBs [47,48] and consequently, UFG is obtained. After the 4th MMSECAP pass, the structure exhibits both elongated grains and equiaxed grains. A relatively equiaxed grain structure (grain size of ~ 160 nm) can be detected, (Figure 4(b)).

Figure 5 depicts the EBSD grain boundaries map along a section parallel to the extrusion direction and the statistical variations of both the grain size and the boundary misorientation angle distribution for both the 'Undeformed + Extr.' which represents the CG structure and 'Undeformed + ECAP + Extr.' which represents the FG structure. It can be shown that the grain structure of the 'Undeformed + Extr.' consists of a majority of the grains which are displayed along the extrusion direction with an average grain size of ~ 24.6 µm. Moreover, the microstructure consists mainly of LAGBs (84%) with an average misorientation angle of 10.29°, i.e. < 15°, see Figure 5(a,d).

Whereas, the grain structure of the 'Undeformed + ECAP + Extr.' exhibits elongated grain arrangements along with equiaxed ultrafine grains (see Figure 5(b)). The relatively large elongated grains are observed as distributed intermittently measuring about 13 µm (see Figure 5(c)). Additionally, Figure 5(c) shows that the mean grain size for 'Undeformed + ECAP + Extr.' is about 2.5 µm, and 30% of the scanned area exhibited grains less than 1.5 µm. Additionally, it is observed that the microstructure of the 'Undeformed + ECAP + Extr.' specimen mainly consists of HAGBs (65%) indicating that some LAGBs have been transformed into HAGBs after MMSECAP by the extrusion process as shown in Figure 5(d).

Deformation characteristics of MIU process

Figure 6 shows the load–stroke curves of the two different structures, i.e. CG and FG after the upsetting test. It is worth noting that each curve was drawn from the average of 20 points from the data obtained to give one point. It is found that the deformation load of the Undeformed + ECAP + Extr. has a higher value than that of Undeformed + Extr. This can be ascribed to two factors, i.e. grain boundary strengthening and the change

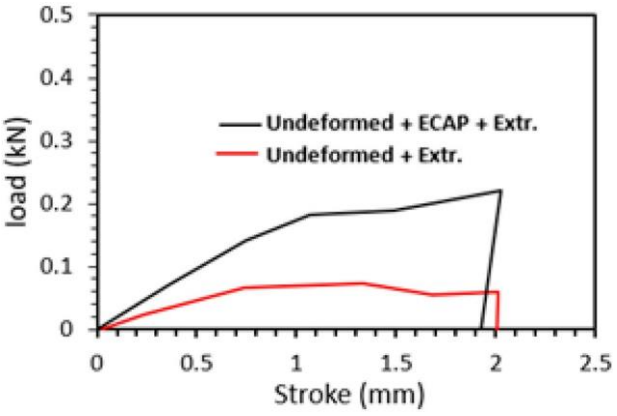

Figure 6. Load-stroke curves of Al 1070 alloy processed during injection upsetting test.

of surface grain fraction. The former can be described by Hall–Petch relation in which the material flow stress increases with the inverse of the square root of the grain size follow [49,50]. Whereas, the latter can be explained by the sense that the grains existing on the surface have less constraint, and thus, their flow stress is lower than that of the interior grains [51].

The microstructure of the Al 1070 specimens obtained by electron backscattered diffraction mapping at the centre region of the upsetted surface for the Undeformed + Extr., and Undeformed + ECAP + Extr., can be observed in Figure 7(a,b). Figure 7(c,d) depicts the corresponding grain size distribution. The results display that the average grain sizes of the upsetted specimens were 13.29 and 2.02 μm for FG and CG structure, respectively. It is depicted that 85%of the scanned zone of the Undeformed + Extr. had grains more than 4 μm in diameter, Figure 7(c). Whereas 85% of the scanned zone of the Unde- formed + ECAP + Extr. had grains less than 4 μm andthe microstructure shows a homogenous distribution for the deformed grains (Figure 7(d)).

Figure 8 shows SEM images for Al 1070 alloyon the edge surface after the micro-upsetting test. The micro-upsetted edge for the Undeformed + Extr. has severe cracks that formed and propagated along the surface. Nevertheless, the surface quality of the micro-upsetted progressively improved from CG to FG structure. Since the micro-upsetting of the Undeformed + ECAP + Extr. structure has a good form-accuracy and is free of undesirable defects such as edge cracking.

Such differences in the grain size affect the anisotr opy during the upsetting test for the deformed shape. Figure 9 demonstrates the surface topographies of the end surface of the upsetted specimens for both the two different grain structures. The inspection shows that the geometries of the upsetted specimen have more irregularities around the perimeter and the surface profileis not circular for the Undeformed + Extr. as demonstrated in Figure 9 (a1, a2). This could be attributed to the anisotropy properties of individual grains, i.e. the shape of the grains at the surface. Whereas, the outer shape of the Undeformed + ECAP + Extr. is appeared very smooth exhibiting regular sidewall around the perimeter (see Figure 9 (b1, b2)). Besides, the end surface has more circularity when the deformed specimen contains several grains, and this affects the deformation shape that was significantly improved with decreasing the grain size.

From these observations, it is concluded that the grain size affects the material deformation behaviour on the micro-scale. This is in an agreement with the results reported by Chan et al. [43] since they observed inhomogeneous deformation taken place with increasing the grain size and decreasing the speci-men size by employing micro-compression for Al-6061alloy.

In the high magnification of the end surface, Figure 9 (a2, b2), it is observed that there is an outer rim at the end surface of the upsetted specimens in dark areas called the real contact area (RCAs).

Figure 10(a) shows clearly the end-surface representation of the upsetted specimen in the case of CG specimen by using a laser microscope. The light areas in Figure 10(a) are actually the RCAs, while the dark areas are the closed pocket (CPs). It is found that the RCAs are located at the outer rim of the end surface, whereas the CPs are more concentrated at the inner region of the specimen. In the upsetting test, materi- als flow outwards when it is compressed and the end surface expands radially. It is known that the material has some asperities that contain valleys and peaks on its surface. When the specimen is pressed against the TiN plate, some of the asperities that have the highest peaks deform and become flat, thus resulting in an increase in the RCAs and interfacial friction [52]. Meanwhile, the asperity valleys led to the formation of a close pocket (CPs). Eventually, the small CPs coalesce to form a large CP at the inner area of the end surface. This can be clarified by the characteristics of the material surface in the metal forming process, i.e. interfacial friction.

Hence, it is interesting to estimate the friction factor for both CG and FG upsetted specimens. When a cylindrical specimen is axially compressed between a top and a bottom plate, the specimen material in contact with their surfaces experiences heterogeneous deformation resulting in the occurrence of the barrelled side profile, this being shown in Figure 10(b). This is due to the interfacial friction at the faces of contact that slows down the flow of metal on the surface and in its vicinity during deformation, whereas the rest of the specimen exhibiting high strains and bulges out. Thus, it is essential to evaluate a friction factor for bulging. The friction factor (m) was measured by using Ebrahimi and Najafizadeh analysis [53], proceeding from the upper bound theorem and the geometry of

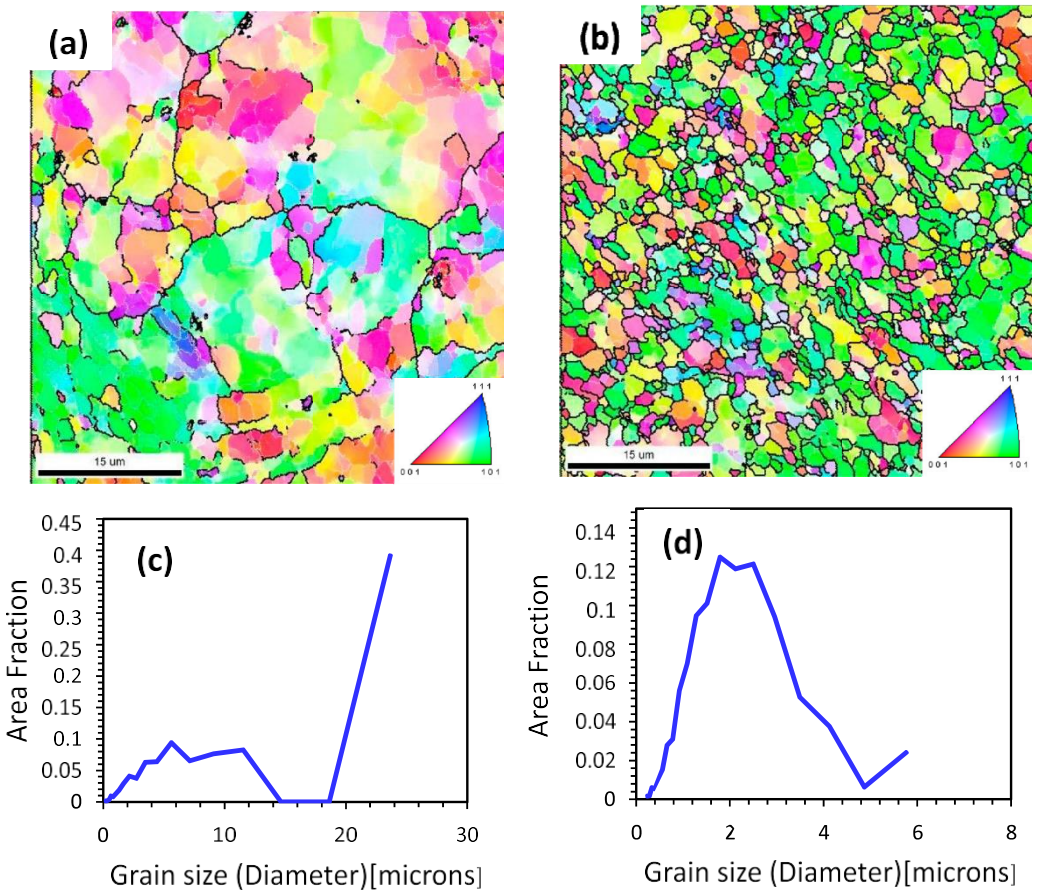

Figure 7. Microstructures of the specimens processed by injection upsetting: (a) Undeformed + Extr.,(b) Unde-formed + ECAP + Extr., and (c,d) are the corresponding statistical variation of grain size.

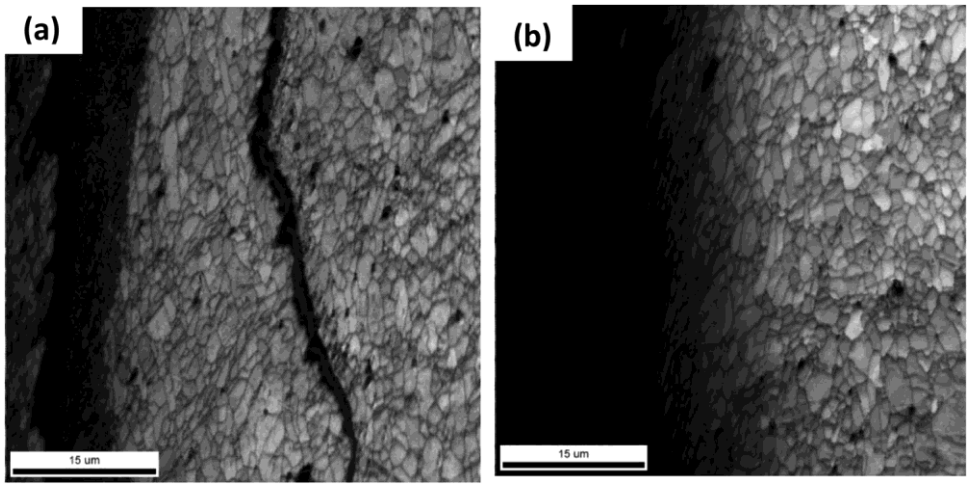

Figure 8. SEM images of the micro-upsetting for Al1070 alloy: (a) CG and, (b) FG material. Defects such as edge-cracks are clearly visible on the edge surface in the case of CG structure.

the testing specimen. The friction factor is given by the following equation:

$$m = \frac{\sqrt{(R/H)b}}{4/\sqrt{3} - 2b/3\sqrt{3}} \quad (1)$$

where R and H are the average radius and height of the upsetted specimen, and b is the barrelling param- eter. R and b can be determined by the following equations:

$$R = R_0 \sqrt{\frac{H_0}{H}} \quad (2)$$

$$b = 4\frac{\Delta R}{R}\frac{H}{H_0 - H} \quad (3)$$

where R_0 and H_0 are the initial radius and the specimen height, respectively. The difference between mid-height radius (R_M) and bottom radius (R_b) is defined

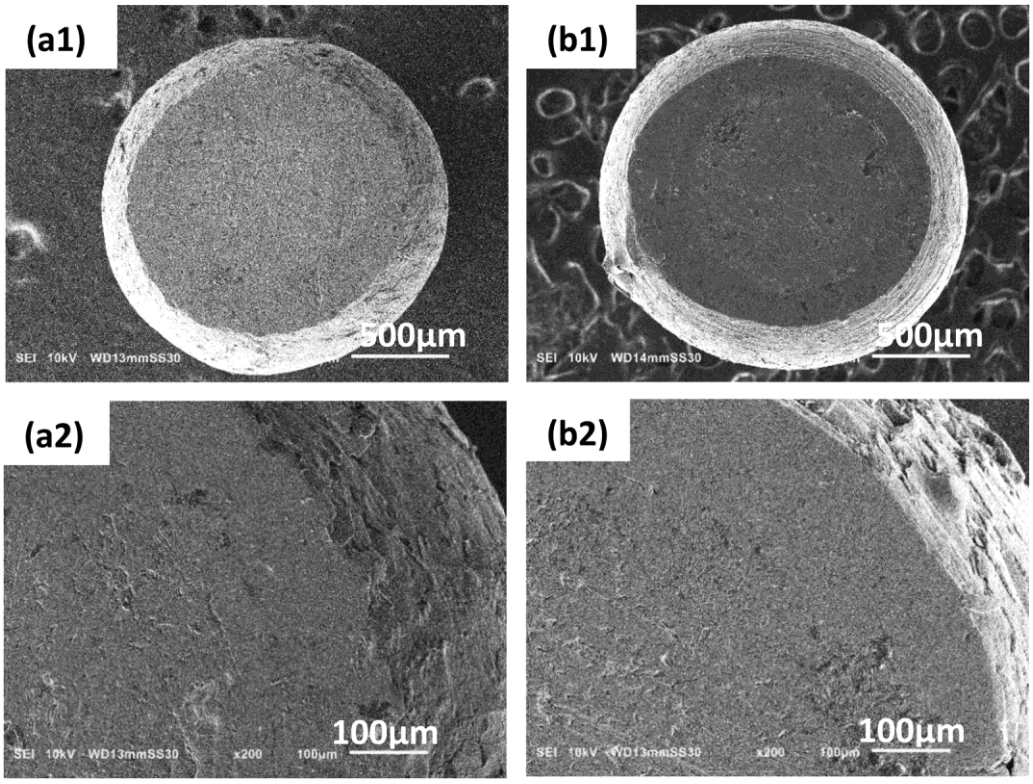

Figure 9. Low (a1, b1) and high (a2, b2) magnification SEM images showing the surface topographies of the upsetted specimens where 'a' represent the CG and 'b' represents the FG. The end surfaces of (b, FG) have a better surface quality compared with the CG counterpart.

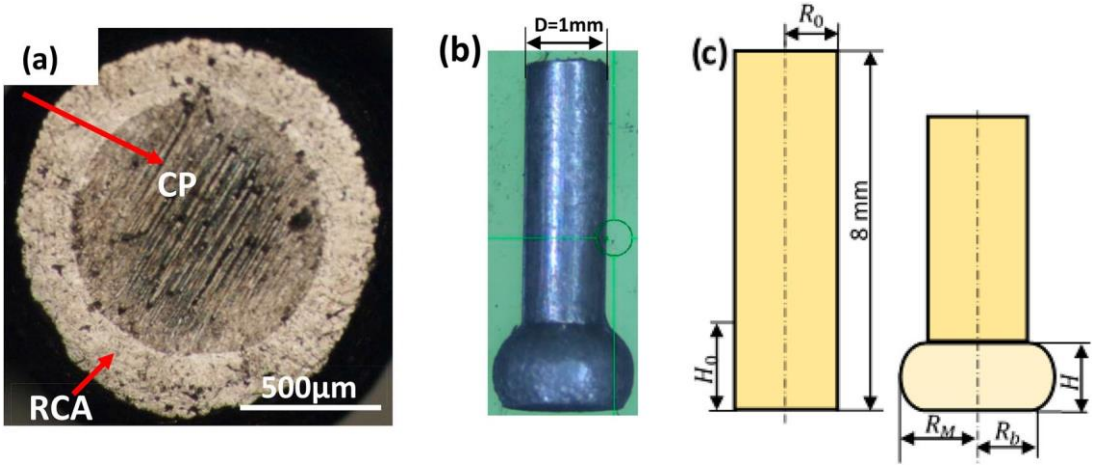

Figure 10. (a) End-surface topography of the upsetted specimen in the case of the annealed state, (b) typical appearance of the specimen after MIU process, and (c) geometrical representation of upsetting specimen.

as ΔR. Practically, the precise measurement of the bottom radius of the cylinder after deformation is difficult. Hence, an approximation of the shape of the barrelled specimens with an arc of a circle, R_b can be estimated by the following equation:

$$R_b = \sqrt{3\frac{H_0}{H}R_0^2 - 2R_M^2} \quad (4)$$

The calculated value of the friction factor from the aforementioned equations for CG and FG structure is shown in Figure 11. It is observed that the friction factor is higher in the case of the FG structure. This is in a line with the prior studies [52,54] in which the friction factor increases with decreasing the grain size and this can be ascribed to the change of mate- rial properties. Since the material flow stress during deformation is decreased with the increasing grain size. This is because the volume fraction of grain boundaries decreases with increasing grain size [55]. Further, the flow stress for surface grains which have less constraint to flow becomes substantial to the overall deformation behaviour [56]. Thus, the material can flow outwards easily and lead to an increase in the end surface area.

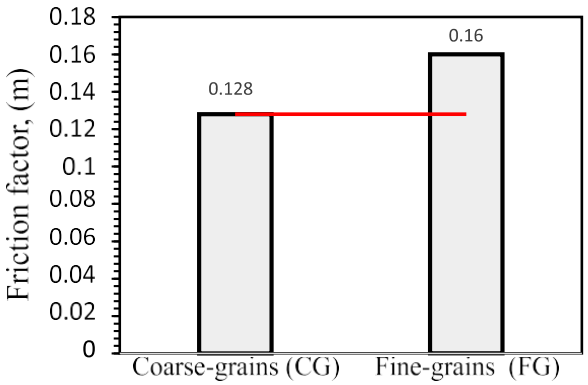

Figure 11. The variation of friction factor with two differentgrain structures, i.e. CG and FG.

Conclusion

In this research, Al 1070 alloy was processed by the MMSE on two different grain structures, coarse grain (CG) and fine grain (FG) obtained by the 4th pass of MMSECAP using route Bc. Then the extruded tiny pins were tested for their formability and plastic flow via the injection upsetting. The key conclusions are drawn as follows:

(1) After the 4th pass of MMSECAP, the average grain size was refined from ~ 20 μm to ~ 2 μm, and also the microstructure exhibited UFG of 160 nm. The higher degree of grain refinement of the processed aluminuim alloy by the MMSECAP is ascribed to the mechanism of grain subdivision.

(2) Extrusion of the 4th ECAP processed specimen induced a non-uniform microstructure with elongated grain arrangements and further introduced a high fraction of misorientation angle boundaries of about ~65%.

(3) The micro-upsetting of the FG structure has a good form-accuracy and is free of undesirable defects such as edge cracking. Nevertheless, for the CG structure, the quality of micro-upsetted specimens is significantly poorer and has severe cracks that have formed and propagated transversely along the surface.

(4) In the case of the FG structure, the friction factor represented a higher value relative to the CG. This is for the reason that the small grain size triggered a higher volume fraction of grain boundaries that lead to increasing the flow stress for surface grains.

(5) Finally, this study suggests that the FG structure materials for microforming processing to fabricate micro-components which can, in turn, be applied in MEMS.

Disclosure statement

No potential conflict of interest was reported by the author(s).

Funding

The authors would like to acknowledge the financial support from the Missions Sector-Higher Education Ministry, Egypt, through this work.

References

[1] Geiger M KM, Eckstein R, Tiesler N, et al. Microforming. CIRP Ann. 2001;50(2):445–462.
[2] Vollertsen F, Niehoff HS, Hu Z. State of the art in micro forming. Int J Mach Tools Manuf. 2006;46(11):1172–1179.
[3] Dhal A, Panigrahi S, Shunmugam M. Achieving excellent microformability in aluminum by engineering a unique ultrafine-grained microstructure. Sci Rep. 2019;9(1):10683.
[4] Xu J, Guo B, Shan D, et al. Development of a microforming system for micro-punching process of microhole arrays in brass foil. J Mater Process Technol. 2012;212(11):2238–2246.
[5] Xu J, Li J, Shi L, et al. Effects of temperature, strain rate and specimen size on the deformation behaviors at micro/meso-scale in ultrafine-grained pure Al. Mater Charact. 2015;109:181–188.
[6] Fu M, Chan W. A review on the state-of-the-art microforming technologies. Int J Adv Manuf Technol. 2013;67(9–12):2411–2437.
[7] Vollertsen F, Biermann D, Hansen HN, et al. Size effects in manufacturing of metallic components. CIRP Ann. 2009;58(2):566–587.
[8] Xu J, Zhu X, Shan D, et al. Effect of grain size and specimen dimensions on micro-forming of high purity aluminum. Mater Sci Eng A. 2015;646:207–217.
[9] Chan W, Fu M, Lu J. Experimental and simulation study of deformation behavior in micro-compound extrusion process. Mater Des. 2011;32(2):525–534.
[10] Janssen P, De Keijser TH, Geers M. An experimental assessment of grain size effects in the uniaxial straining of thin Al sheet with a few grains across the thickness. Mater Sci Eng A. 2006;419(1–2):238–248.
[11] Wang C, Shan D, Zhou J, et al. Size effects of the cavity dimension on the microforming ability during coining process. J Mater Process Technol. 2007;187: 256–259.
[12] Rosochowski A, Presz W, Olejnik L, et al. Microextrusion of ultra-fine grained aluminium. Int J Adv Manuf Technol. 2007;33(1–2):137–146.
[13] Ast J, Durst K. Nanoforming behaviour and microstructural evolution during nanoimprinting of ultrafine-grained and nanocrystalline metals. Mater Sci Eng A. 2013;568:68–75.
[14] Kim W, Yoo S, Kim H. Superplastic microforming of Mg–9Al–1Zn alloy with ultrafine-grained microstructure. Scr Mater. 2008;59(6):599–602.
[15] Xu J, Shirooyeh M, Wongsa-Ngam J, et al. Hardness homogeneity and micro-tensile behavior in a magnesium AZ31 alloy processed by equal-channel angular pressing. Mater Sci Eng A. 2013;586:108–114.
[16] Schneibel J, Heilmaier M, Blum W, et al. Temperature dependence of the strength of fine- and ultrafine-grained materials. Acta Mater. 2011;59(3): 1300–1308.
[17] Le G, Godfrey A, Hansen N, et al. Influence of grain size in the near-micrometre regime on the defor- mation microstructure in aluminium. Acta Mater. 2013;61(19):7072–7086.

[18] Warthi N, Ghosh P, Chokshi AH. Approaching theoretical strengths by synergistic internal and external size refinement. Scr Mater. 2013;68(5):225–228.
[19] Bryła K, Horky J, Krystian M, et al. Microstructure, mechanical properties, and degradation of Mg-Ag alloy after equal-channel angular pressing. Mater Sci Eng: C. 2020;109:110543.
[20] Dyakonov G, Mironov S, Semenova I, et al. EBSD analysis of grain-refinement mechanisms operating during equal-channel angular pressing of commercial-purity titanium. Acta Mater. 2019;173:174–183.
[21] Vaughan M, Samimi P, Gibbons S, et al. Exploring performance limits of a new martensitic high strength steel by ausforming via equal channel angular pressing. Scr Mater. 2020;184:63–69.
[22] Abdelaziem W, Hamada AS, Hassan MA. Effect of the cyclic extrusion and compression processing on microstructure and mechanical properties of Al-1%Cu alloy. Key Eng Mater. 2018;780:93–97. Trans Tech Publ.
[23] Lin J, Wang Q, Peng L, et al. Microstructure and high tensile ductility of ZK60 magnesium alloy processed by cyclic extrusion and compression. J Alloys Compd. 2009;476(1–2):441–445.
[24] Zhang Y, Jin S, Trimby PW, et al. Dynamic precipitation, segregation and strengthening of an Al-Zn-Mg-Cu alloy (AA7075) processed by high-pressure torsion. Acta Mater. 2019;162:19–32.
[25] Castro MM, Sabbaghianrad S, Pereira PHR, et al. A magnesium-aluminium composite produced by high-pressure torsion. J Alloys Compd. 2019;804: 421–426.
[26] Abdel-Aziem W, Hamada A, Makino T, et al. Micro/Meso-scale equal channel angular pressing of Al 1070 alloy: microstructure and mechanical properties. J Mater Eng Perform. 2020;29(9):6201–6211.
[27] Abdel-Aziem W, Hamada A, Makino T, et al. Microstructural evolution during extrusion of equal chan- nel angular-pressed AA1070 alloy in micro/mesoscale. Mater Sci Technol. 2020: 1–9.
[28] Abdel-Aziem W, Hamada A, Makino T, et al. Microstructure Evolution of AA1070 Aluminum Alloy Processed by Micro/Meso-Scale Equal Channel Angular Pressing. Met Mater Int. 2019: 1–13.
[29] Sun P-L, Kao P-W, Chang C-P. Effect of deformation route on microstructural development in aluminum processed by equal channel angular extrusion. Metall Mater Trans A. 2004;35(4):1359–1368.
[30] Abdel-Aziem W, Hassan MA, Makino T, et al. Microstructure, Mechanical Properties of Extruded Aluminum at Different Ram Speeds in Micro/Meso-Scale. Metallog, Microstruct Anal. 2021: 1–8.
[31] Hansen N, Huang X, Winther G. Effect of grain boundaries and grain orientation on structure and properties. Metall Mater Trans A. 2011;42(3):613–625.
[32] Winther G, Huang X, Hansen N. Crystallographic and macroscopic orientation of planar dislocation boundaries—correlation with grain orientation. Acta Mater. 2000;48(9):2187–2198.
[33] Liu Q, Hansen N, Maurice C, et al. Heterogeneous microstructures and microtextures in cube-oriented al crystals after channel die compression. Metall Mater Trans A. 1998;29(9):2333–2344.
[34] Ma Q, Mao W, Li B, Wang P and Horstemeyer M. Grain subdivision and its effect on texture evolution in an aluminum alloy under plane strain compression in Light metals 2013. Springer; 2016, p. 351–356.
[35] Hurley P, Humphreys F. The application of EBSD to the study of substructural development in a cold rolled single-phase aluminium alloy. Acta Mater. 2003;51(4): 1087–1102.
[36] Hurley P, Bate P, Humphreys F. An objective study of substructural boundary alignment in aluminium. Acta Mater. 2003;51(16):4737–4750.
[37] Humphreys F, Prangnell P, Bowen JR, et al. Developing stable fine–grain microstructures by large strain deformation. Philos Trans R Soc , A. 1999;357(1756):1663–1681.
[38] Beyerlein I, Lebensohn R, Tome C. Modeling tex-ture and microstructural evolution in the equal chan- nel angular extrusion process. Mater Sci Eng A. 2003;345(1–2):122–138.
[39] Yang G, Li Z, Yuan Y, et al. Microstructure, mechanical properties and electrical conductivity of Cu–0.3Mg–0.05Ce alloy processed by equal channel angular pressing and subsequent annealing. J Alloys Compd. 2015;640:347–354.
[40] Sun P, Kao P, Chang C. High angle boundary formation by grain subdivision in equal channel angular extrusion. Scr Mater. 2004;51(6):565–570.
[41] Roodposhti PS, Farahbakhsh N, Sarkar A, et al. Microstructural approach to equal channel angular processing of commercially pure titanium – a review. Trans Nonferrous Met Soc China. 2015;25(5):1353–1366.
[42] Semenova I, Polyakov A, Raab G, et al. Enhanced fatigue properties of ultrafine-grained Ti rods processed by ECAP-Conform. J Mater Sci. 2012;47(22):7777–7781.
[43] Xirong Y, Xicheng Z, Wenjie F. Deformed microstructures and mechanical properties of CP-Ti processed by multi-pass ECAP at room temperature. Rare Met Mater Eng. 2009;38(6):955–957.
[44] Delannay L, Mishin O, Jensen DJ, et al. Quantitative analysis of grain subdivision in cold rolled aluminium. Acta Mater. 2001;49(13):2441–2451.
[45] Bay B, Hansen N, Hughes D, et al. Overview no. 96 evolution of f.c.c. deformation structures in polyslip. Acta Metall Mater. 1992;40(2):205–219.
[46] Kuhlmann-Wilsdorf D. Theory of plastic deformation: properties of low energy dislocation structures. Mater Sci Eng A. 1989;113:1–41.
[47] Kaibyshev R, Shipilova K, Musin F, et al. Continuous dynamic recrystallization in an Al–Li–Mg–Sc alloy during equal-channel angular extrusion. Mater Sci Eng A. 2005;396(1–2):341–351.
[48] Liao X, Huang J, Zhu Y, et al. Nanostructures and deformation mechanisms in a cryogenically ball-milled Al-Mg alloy. Philos Mag. 2003;83(26):3065–3075.
[49] Hansen N. Hall–Petch relation and boundary strengthening. Scr Mater. 2004;51(8):801–806.
[50] Kusakin P, Belyakov A, Molodov DA, et al. On the effect of chemical composition on yield strength of TWIP steels. Mater Sci Eng A. 2017;687:82–84.
[51] Fu MW and Chan WL. Micro-scaled products development via microforming, series in advanced manufacturing. London: Springer; 2014.
[52] Deng J, Fu M, Chan W. Size effect on material surface deformation behavior in micro-forming process. Mater Sci Eng A. 2011;528(13):4799–4806.
[53] Ebrahimi R, Najafizadeh A. A new method for evaluation of friction in bulk metal forming. J Mater Process Technol. 2004;152(2):136–143.
[54] El-Raghy T, Blau P, Barsoum MW. Effect of grain size on friction and wear behavior of Ti3SiC2. Wear. 2000;238(2):125–130.

[55] Chan W, Fu M, Lu J, et al. Modeling of grain size effect on micro deformation behavior in micro-forming of pure copper. Mater Sci Eng A. 2010;527(24–25):6638–6648.

[56] Chan W, Fu M, Lu J. The size effect on micro deformation behaviour in micro-scale plastic deformation. Mater Des. 2011;32(1):198–206.